Available online at www.sciencedirect.com
ScienceDirect
Nuclear Instruments and Methods in Physics Research A 571 (2007) 612–621
NUCLEAR INSTRUMENTS & METHODS IN PHYSICS RESEARCH Section A
www.elsevier.com/locate/nima

Beam test of a full-length prototype of the BESIII drift chamber with the readout electronics

Z.H. Qin[a,b,*], Y.B. Chen[a], H.Y. Sheng[a], L.H. Wu[a,b], J.B. Liu[a,b], B.A. Zhuang[a], X.S. Jiang[a], Y.B. Zhao[a], K.J. Zhu[a], Z.K. Yan[a,c], C. Chen[a], M.H. Xu[a], L. Wang[a], X.Y. Ma[a], X. Tang[a], R.G. Liu[a], Y. Jin[a], Q.M. Zhu[a], G.F. Zhang[a], Z. Wu[a,b], R.Y. Li[a], P.P. Zhao[a], H.L. Dai[a], X.P. Li[a], J. Li[a]

[a]*Institute of High Energy Physics, CAS, Beijing 100049, China*
[b]*Graduate School of the Chinese Academy of Sciences, Beijing 100049, China*
[c]*Micro-electronics Laboratory, Department of Physics, Hunan University, Changsha 410082, China*

Received 28 September 2006; received in revised form 6 November 2006; accepted 6 November 2006
Available online 1 December 2006

Abstract

A full-length prototype of the BESIII drift chamber together with its readout electronics was built and a beam test was performed. Two different methods, namely "single-threshold method" and "double-threshold method" for timing measurement, were studied. Test results show that the BESIII drift chamber and its readout electronics can reach their design specifications. The "double-threshold method" results in a better timing accuracy and noise suppression capabilities as compared with the "single-threshold method".

PACS: 29.40.Gx

Keywords: BESIII; Drift chamber; Prototype; Readout electronics; Resolution; Beam test; Threshold

1. Introduction

The BESIII experiment [1] at the upgrading Beijing Electron Positron Collider (BEPCII) with an energy range of 2–5 GeV, a peak luminosity of $10^{33}\,cm^{-2}\,s^{-1}$ at 3.78 GeV [2] is designed for high-precision measurements and new physics searches in the τ-charm energy region. The BESIII tracking chamber, occupying the radial extent from 53 to 810 mm with 43 sense wire layers and the axial extent of 2.3 m long, adopts the small drift-cell design using low Z field wires filled with helium-based operating gas to provide a single hit efficiency of better than 98%, a solid-angle coverage up to 90% 4πSr, a spatial resolution better than 130 μm averaged over all cells, a dE/dx resolution better than 6% for π/K separation up to a momentum of 700 MeV/c, and a transverse momentum resolution of about 0.5% at 1 GeV/c.

The readout electronics for the BESIII drift chamber is designed to measure the drift time and charge with a high precision [1]. The time measurement is implemented by a High-Performance TDC chip, called HPTDC, and developed by the CERN microelectronics group [3]. The required time resolution is better than 0.5 ns, which delivers a negligible contribution to positioning since the average drift velocity is 30 μm/ns. The integral non-linearity for time measurement is designed to be less than 0.5%. The charge measurement is based on a flash ADC (hereafter called FADC) with a digital pipeline. The designed resolution is better than 8 fc and the required integral non-linearity is less than 2%. The BEPCII collider will run in a multi-bunch mode with the bunch spacing of 8 ns and the Level 1 trigger latency of 6.4 μs, the expected wire-by-wire hit rate is about 30 kHz and the estimated Level 1 trigger rate is up to 4 kHz; hence the readout electronics

*Corresponding author. Institute of High Energy Physics, CAS, Beijing 100049, China. Tel.: +8610 88236069; fax: +8610 88236423.
E-mail address: qinzh@mail.ihep.ac.cn (Z.H. Qin).

0168-9002/$ - see front matter © 2006 Elsevier B.V. All rights reserved.
doi:10.1016/j.nima.2006.11.032

adopts a least dead-time design based on the techniques of pipeline, zero suppression and multi-stage parallel processing. In addition, two different methods of the electronics thresholds for timing measurement are investigated.

A full-length prototype of the BESIII drift chamber together with a set of readout electronics was built A beam test was carried out at the E3 beam line at IHEP [4] to study the performance of the prototype chamber and the readout electronics and to determine the threshold method for the timing measurement. In the following sections, the prototype, the readout electronics and data acquisition system, and the test beam layout are described. The test results, covering drift time distribution, x–t relation, spatial resolution, dE/dx measurements and cell efficiency are presented and discussed in detail. A conclusion of the beam test is given at the end.

2. The full-length prototype

The full-length prototype reproduces the radial extent of the BESIII drift chamber from 505 to 740 mm, with an azimuthal width of 0.5 m and an axial length of 2.2 m. Fig. 1 shows its structure, which is composed of two endplates, four lateral plates, and two end-placed boxes for shielding of the front-end electronics. These components are all made of aluminum and the two endplates are precisely assembled via four well-machined aluminum rods. There is a $6 \times 6\,cm^2$ mylar window for beam particles incidence located at the center of the two lateral plates perpendicular to the beam direction. A total of 158 gold-plated tungsten (3% rhenium) sense wires, 25 μm in diameter, and 572 gold-plated aluminum field wires, 110 μm in diameter, are strung inside the prototype chamber. Feedthroughs with the copper and aluminum crimp pins, crimped manually, are used to fix the sense wires and field wires, respectively.

Fig. 2 exhibits the cell structure and wire layers arrangement of the full-length prototype, viewed along the Z direction at the central plane of the prototype. The 158 drift cells, each with a nearly squared shape and a half-cell width of 8.1 mm, are disposed in 14 concentric layers with two boundary layers for layers 1 and 14, three super-layers including one axial super-layer for layers 10–13, and two stereo super-layers for layers 6–9 and 2–5 alternating in stereo directions of "left" and "right". The magnitude of the stereo angle is about 52 mrad. The neighboring layers in one super-layer are staggered by half of a cell to resolve the left-right ambiguity. In order to reduce the left-right asymmetry of x–t relations in the boundary layers, an additional field wire layer with the number of wires corresponding to the larger radius super-layer, is arranged between the axial super-layer and the stereo super-layer [5].

The operating gas of the prototype is a mixture of Helium/C_3H_8 (60/40), the same as that to be adopted by the BESIII drift chamber, with a flow rate of about one volume ($\approx$400 l) exchange per day. The gas system runs in a continuous flushing mode keeping the operating pressure about 2 mbar above the atmospheric pressure. An MKS mass flow meter (type 1259B) is used to control the gas flow rate.

The high voltage system for the prototype is also same as that for the BESIII drift chamber [6]. Totally 18 channels of high voltage, provided by CAEN HV power supply of SY127 [7], are equipped for the prototype with 14 channels supplied to the sense wire layers and the other 4 channels to the field wires located in boundary layers to reduce the left-right asymmetry of the x–t relation [8]. Each channel of the high voltage, after provided by the SY127, is fed to a distribution board composed of several separated distribution cards. And, after fanned out by these cards, the high voltage is sent to a HV board. One HV board is connected to 8 sense wires through a shielded wire of several centimeters long. The high voltage value for the sense wires is about 2200 V while for the field wires is about 200 V.

3. Readout electronics and data acquisition system

The readout electronics equipped for the prototype, is mainly composed of the three components of 23

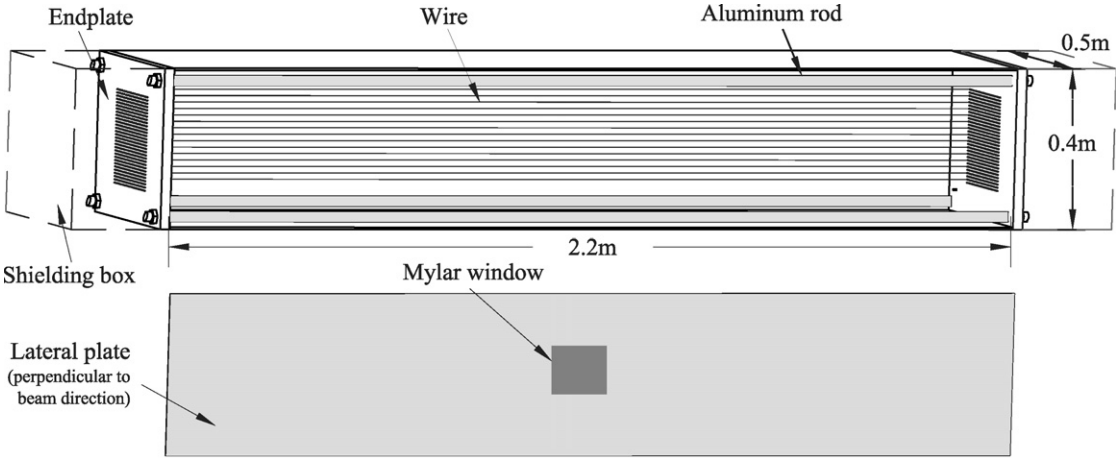

Fig. 1. Schematic view of the full-length prototype of the BESIII drift chamber.

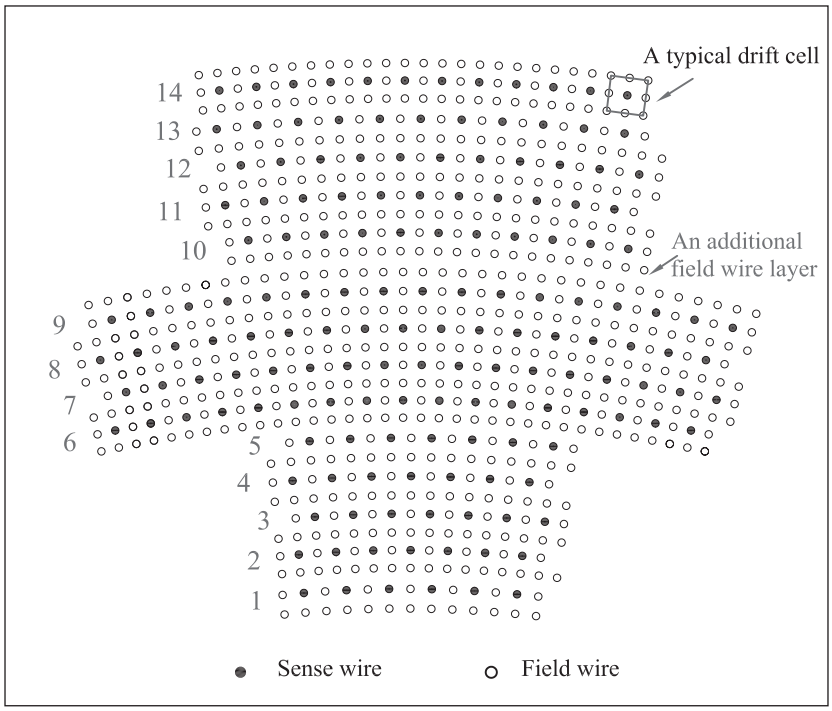

Fig. 2. Cell structure and wire layer arrangement of the prototype, viewed along the Z direction at the central plane of the prototype.

preamplifiers, a 6U and a 9U VME64x crate, which is shown in Fig. 3 together with the data acquisition system and test beam setup. The preamplifier is designed as the trans-impedance type with a rise time of 5 ns and a gain of 12 mV/μA. Each of that covers 8 sense wires and is mounted on the prototype endplates directly. The 6U VME crate consists of the VME controller of PowerPC750, the trigger and clock production modules of CBT-I and CBT-II, the calibration and system control circuit of MCC, and the TDC module. And the 9U VME crate consists of the readout control module of MROC, the fan-out module of MF-II, and the MQT modules. The MQT module is the key part of the electronics system. It receives the output of the preamplifier and carries out the functions of amplification, shaping, discrimination, time measurement and charge measurement. Totally six MQT modules each covering 32 readout channels are equipped in the beam test.

There are two working modes for the electronics system, namely data taking and calibration, which are determined by the MCC module and the latter working mode is mainly used to test if the system works correctly. At the mode of data taking, the MCC receives a series of control signals from CBT-II, such as "clock", "check", "trigger" and "reset", and sends them to the modules of MROC and MF-II to start the system, while at the calibration mode, the MCC generates these control signals by itself. The MF-II module fans out the signals from the MCC and sends them to the MQT to control the time and charge measurements. The drift time measurement is performed by the HPTDC chip operated in its low-resolution mode (i.e. the precision of measurent is 256 ps) using an external reference clock of 40 MHz taken from the accelerator and synchronized to the collision time. The conceptual diagram for HPTDC time extraction is shown in Fig. 4(a). The coarse time counter and a Delay Lock Loop (DLL) perform the measurement of the arrival time of a hit, and the trigger time tag counger is used to record the trigger number. An L1 buffer with a depth of 256 words is used for storing the measured values during trigger latency while the trigger FIFO used for loading the trigger number from the trigger time tag counter. A trigger matching between the L1 buffer and the trigger FIFO is performed when the L1 trigger is active, during which a match window with the width equal to the maximal drift time is opened; thus, the drift time with respect to the L1 trigger can be extracted. The charge measurement is based on an FADC with a digital pipeline, and the charge value is extracted through a numerical integration, its conceptual diagram is shown in Fig. 4(b). The FADC digitizes the input signal in serials with a 10 bit resolution and a 40 MHz clock, meanwhile the digitized data are serially written into the pipeline buffer at the same clock. The length of the pipeline is designed to be 257 cells to avoid losing the interested event since the trigger latency (6.4 μs) is 256 times longer than the clock period (25 ns), and the remaining 1 cell is used to deliver a datum corresponding to pedestal values. Once the L1 trigger is present, the data in the pipeline will be taken out for integration after performing the pedestal substraction, by which the charge carried by the signal is obtained. Upon

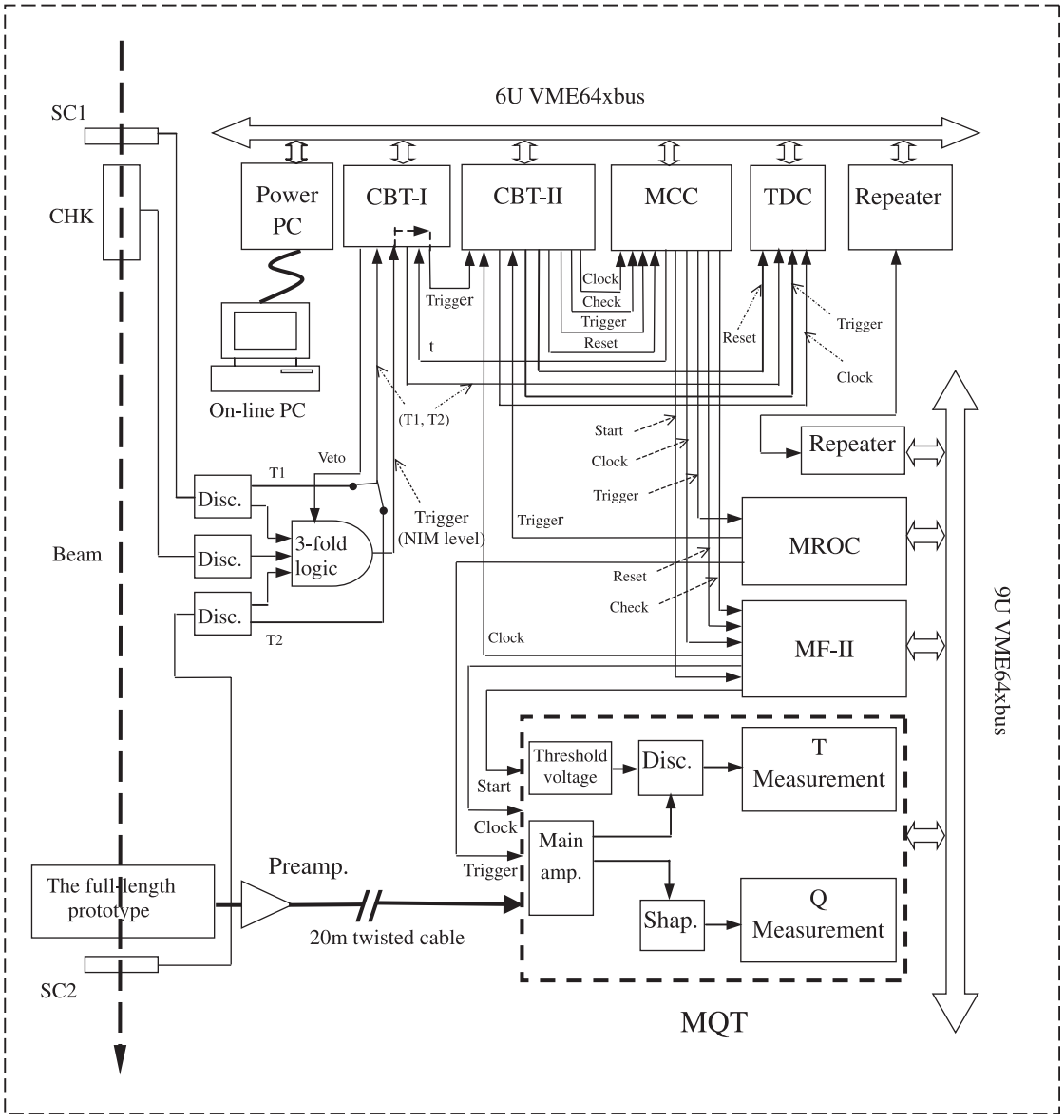

Fig. 3. Block diagram of the readout electronics, data acquisition system and the test beam setup.

the completion for the time and charge measurements, the MROC module will produce an interrupt signal on VME bus, and then data acquisition systme will read out the measured data from the MQT module and deliver them to the on-line PC.

The data acquisition system, used to take the test beam data, is designed for the BESIII experiment [1], adopting the techniques of multi-level buffering, parallel processing, high-speed VME readout and network transmission. Also, running status including the event size, noise level, drift time and charge spectrum is monitored by a program at the online PC to give a real-time information for the whole system.

In the case of beam test, since the 40 MHz clock can't be provided externally, two special-designed modules of CBT-I and CBT-II are used to produce the system clock and to synchronize the NIM level trigger to the clock. Furthermore, a TDC module (also based on HPTDC chip) is required to measure the arrival time of the NIM level trigger. Hence the final drift time is taken from the value measured by MQT subtracting the value measured by TDC. In addition, two different electronic methods are designed in different MQT modules and tested together in the test. For the "double-threshold method", the signal produced by the low threshold discriminator is delayed by 16 ns before coinciding with the signal produced by the high threshold discriminator. Hence, the timing of the input signal is determined by the low threshold while the high threshold can be used for noise suppression. For the "single-threshold method", only one threshold is

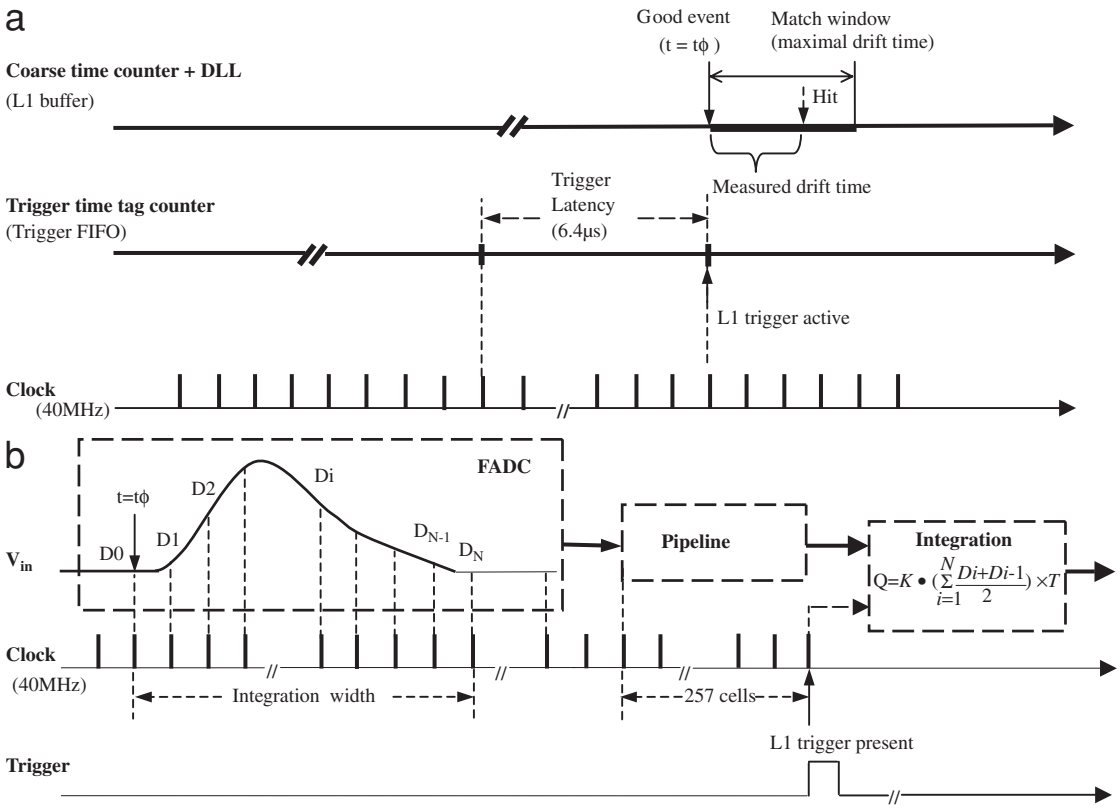

Fig. 4. (a) Conceptual diagram for HPTDC time extraction. (b) Conceptual diagram for numerical integration based on FADC.

designed, for both timing measurement and noise suppression. A detailed comparison of the two methods is performed in terms of the spatial resolution, since which is affected by the timing accuracy.

4. Test beam layout

The beam test of the full-length prototype is performed at the IHEP E3 beam line. Secondary particles such as electron, pion and proton are produced from the BEPC LINAC electron beam on a copper or a beryllium target. The momentum of the beam can be adjusted continuously from 0.2 to 1.1 GeV/c, which almost covers the momentum range for most particles produced at the BESIII experiment. A simplified beam trigger and particle identification system, as shown in Fig. 3, is adopted under a special consideration to reduce the multiple scattering of low-momentum beam particles. Two scintillation counters (SC1–SC2) with a transverse dimension of $8 \times 8\,\mathrm{cm}^2$ were placed 6 m apart along the beam line to provide the trigger as well as the time-of-fight measurement for π/p separation. A threshold Cherenkov counter (CHK), filled with the gas of CO_2, is used to select electrons or positrons. The full-length prototype is placed in the downstream area at the beam line with wire direction perpendicularly to the incident beams. The scintillation counter SC2, placed close to the prototype, is used to determine the T0 for each event (i.e., the time of particles passing through the prototype) at a resolution of better than 200 ps.

5. Results

During the beam test, the low threshold is set at 350 mV, corresponding to a sense wire current of 0.25 μA, while the high threshold is set at 500 mV, the same as that for the "single threshold method", equivalent to a sense wire current of 0.36 μA. Detailed performance test for the prototype and the electronics was carried out at different high voltage settings using the 1.0 GeV/c electrons. Results are discussed in the following sections.

5.1. Drift time distribution

As shown in Fig. 5, a typical drift time distribution is obtained from a single cell indicating that the prototype and the electronics work properly, and the maximal drift time is about 400 ns. The fact that almost no events observed in the region before the leading edge of the distribution shows a very low noise level in the system. The rough T0 for each event can be extracted by fitting the leading edge of the distribution using a formula introduced in Ref. [9].

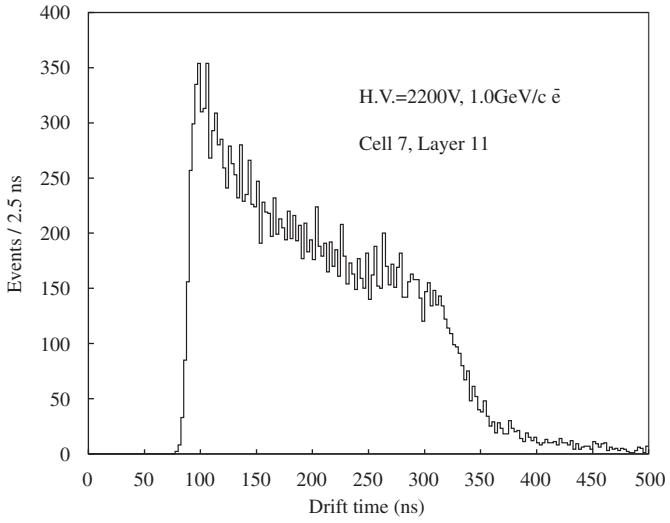

Fig. 5. Typical drift time distribution for a cell.

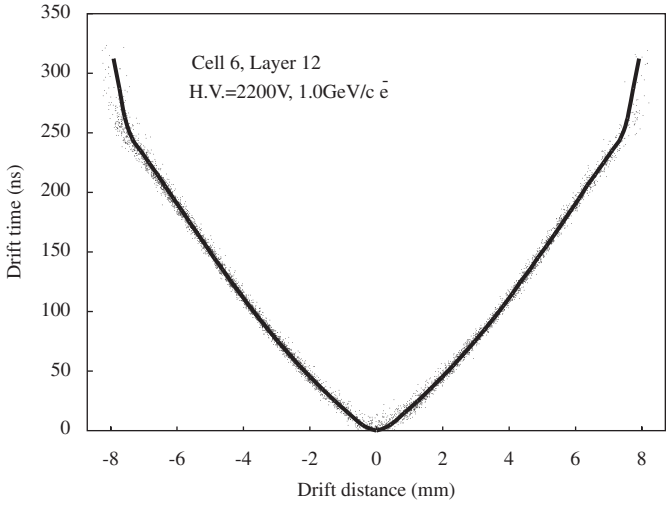

Fig. 6. Scatter plot of the x–t relation for a cell together with the fitted curve.

5.2. x–t relation

The relation of the drift distance to time (x–t relation) is essential to a small-cell drift chamber because of the non-uniformity of the electric field inherent to its cell geometry. The x–t relation is determined layer by layer since there are some differences on the electric field between the layers. Fig. 6 shows the scatter plot of the x–t relation for a single cell together with the fitted curve. The x–t relation is smooth in most regions of the cell but obviously non-linear, with distortions at the boundaries due to the distorted electric field caused by the limited number of field wires and the square-shape cell structure. The x–t relation can be fitted to a fifth order polynomial in the smooth region and to a first order polynomial at the cell boundaries.

5.3. Spatial resolution

The spatial resolution is extracted from the residual distribution of hits with respect to the fitted trajectory of particles after track reconstruction using the final x–t relation. The cell under study is excluded from the track fitting. The error of track fitting is about 5% of the total resolution, and it has been subtracted using a technique described in Ref. [10]. The residual distribution, averaged over all the drift distance, is shown in Fig. 7(a) for cells using the "single threshold method". A dual Gaussian function is used to fit the distribution in order to take into account the tail caused by the cell's non-isochronic charge collection. A spatial resolution of 123 μm is obtained from the residual distribution. The result from the cells using the "double threshold method" is presented in Fig. 7(b). A better spatial resolution of 114 μm is achieved, indicating that the double threshold can improve the accuracy of

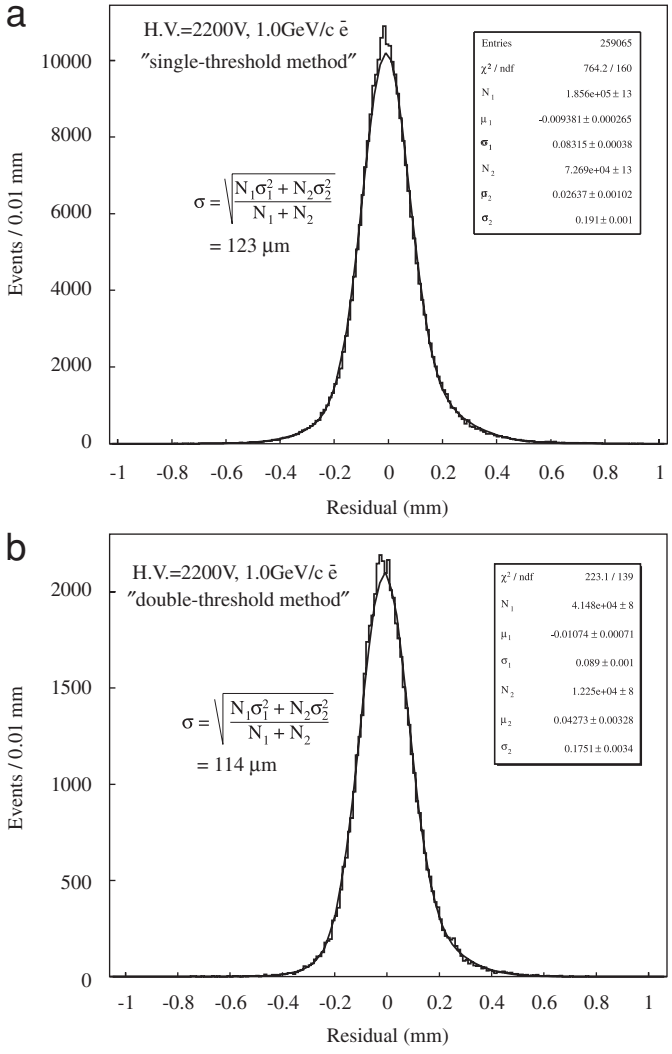

Fig. 7. (a) Average spatial resolution for cells using the "single threshold method" (b) Average spatial resolution for cells using the "double threshold method".

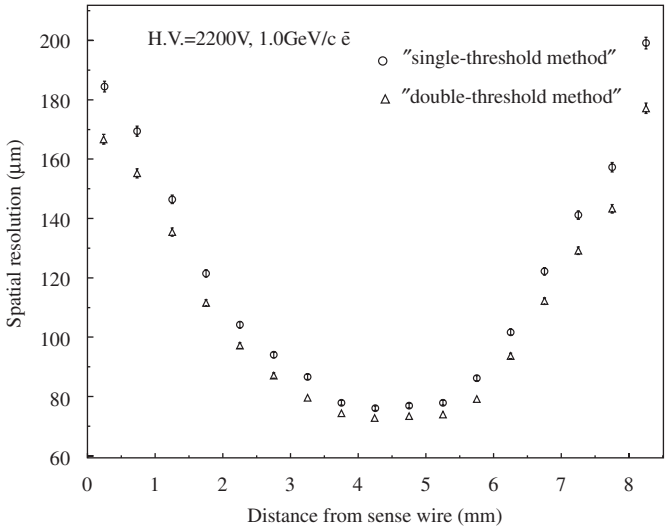

Fig. 8. Spatial resolution as a function of the drift distance, for both the "single threshold method" and the "double threshold method".

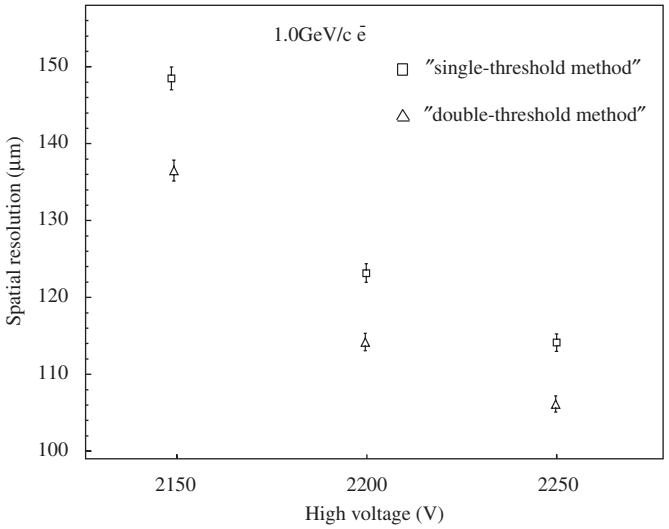

Fig. 9. Average spatial resolution at different operating voltage, for both the "single threshold method" and the "double threshold method".

timing while keeping the noise hit to an acceptable low level.

Fig. 8 shows the spatial resolution as a function of drift distance for the two threshold methods. The spatial resolution deteriorates remarkably near the sense wire due to the fluctuations in the primary ionization, which lead to a severely non-isochronic charge collection. The sharp degradation of the spatial resolution at cell boundaries is due to the distortions of the electric field, which also results in a serious non-isochronic behavior. These are the two primary contributions to the non-Gaussian tail of the residual distribution. A best resolution of about 80 μm is reached at the middle of the cell, which accounts for the narrow Gaussian peak in the residual distribution. For the "double-threshold method", an improvement on spatial resolution is obtained throughout the cell, particularly in regions near the sense wires and cell boundaries.

In ordre to optimize the high voltage setting for the BESIII drift chamber, the spatial resolution at different operating voltages is studied with the beam, as shown in Fig. 9. Increasing the operating voltage can generally result in a larger signal amplitude, hence a smaller time-walk effect and a better spatial resolution, similar to our previous study [11]. Still, the "double-threshold method" gives a better result at all the operating voltages.

5.4. dE/dx measurements

Fig. 10 shows a typical charge spectrum after the pedestal subtraction, for a normal cell with the incident beam of 1.0 GeV/c electrons at a high voltage of 2200 V. The well-known Landau tail is due to the large fluctuation in ionization energy loss induced by charged particles passing through a thin gas volume. The most probable value of the collected charge is about 370 fC, a value larger

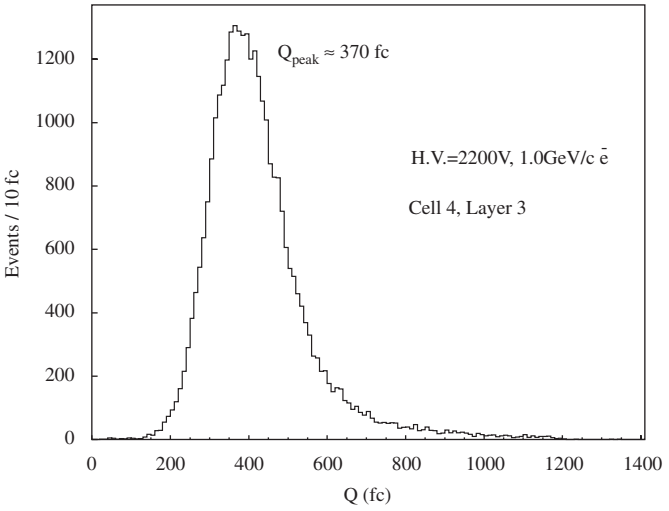

Fig. 10. Typical charge spectrum after pedestal subtraction for a normal cell.

than the energy loss of minimum ionizing particles ($\approx$320 fC), due to the relativistic rise of energy loss for 1.0 GeV/c electrons.

The dE/dx resolution is extracted commonly by a method of truncated mean [12], which averaged the lower dE/dx values at a certain proportion (i.e., the accepted fraction) so that the effect of the Landau tail is weakened and the spectrum of the dE/dx is converted into a Gaussian-like spectrum. In order to perform the measurement with the desired number of samples, the hits from different events are combined to form the fake tracks.

The dE/dx resolution dependence on the accepted fraction is shown in Fig. 11. The best dE/dx resolution is obtained at an accepted fraction of 80%, larger than the case of argon-based gas mixtures. This is because that the smaller Landau tail in He/C_3H_8 (60/40) compensates the

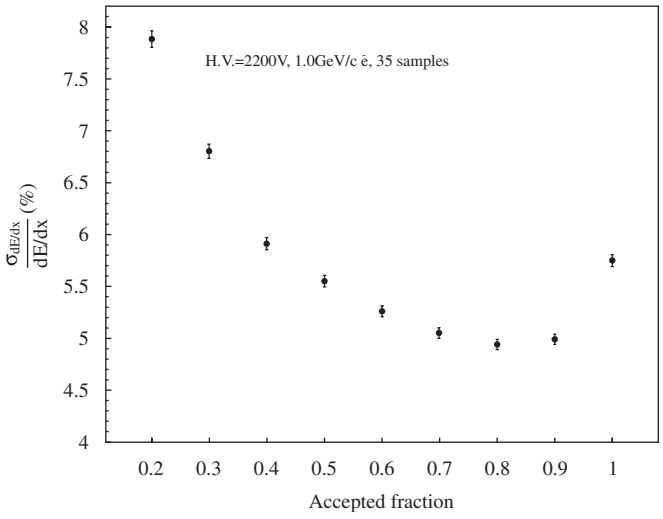

Fig. 11. dE/dx resolution as a function of the accepted fraction.

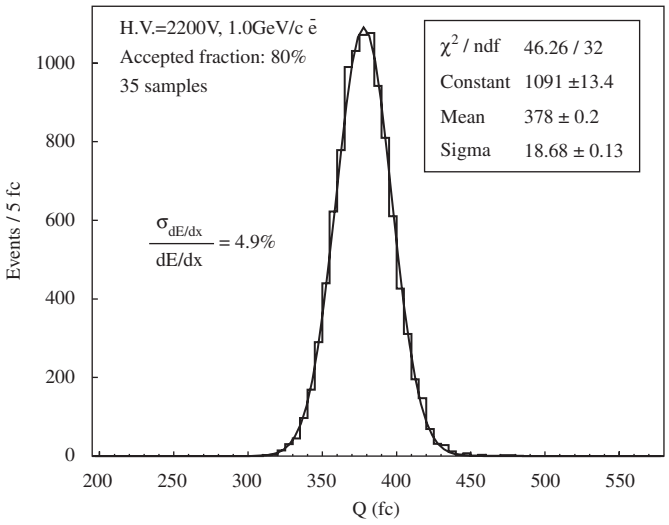

Fig. 13. Truncated mean charge distribution with a simple Gaussian fitting.

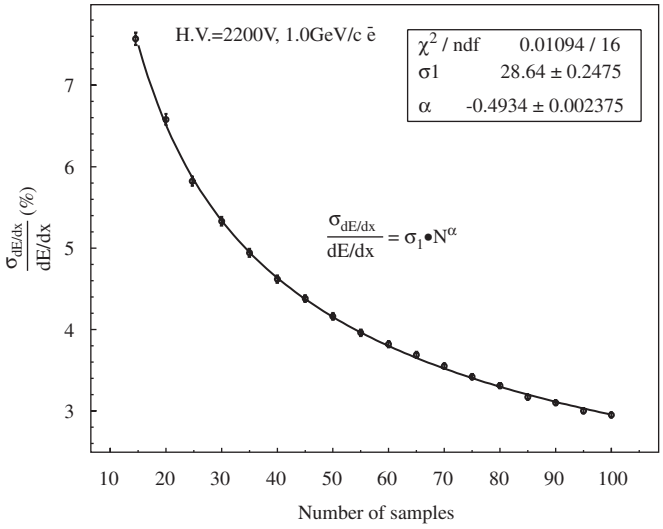

Fig. 12. dE/dx resolution as a function of the number of samples.

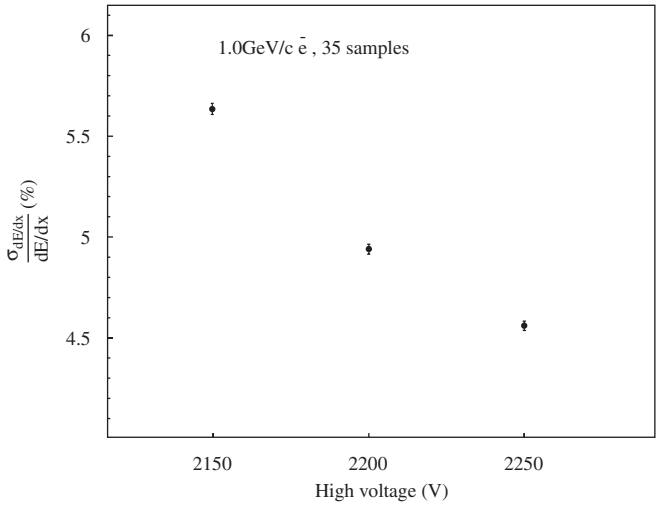

Fig. 14. dE/dx resolution at different operating voltages.

degradation of dE/dx resolution resulted from the smaller number of primary ionization in Helium. Fig. 12 shows the dE/dx resolution as a function of the number of samples. A fit with a power function superimposed to the data, shows that the scaling law is very close to $N^{-0.5}$ as expected from a Gaussian distribution [13], which demonstrates that the Landau tail in the gas mixtures of He/C_3H_8 (60/40) is small. A better dE/dx resolution can be obtained by increasing the number of samples to reduce the fluctuations of energy loss. In case of the BESIII drift chamber (30–40 samples), a dE/dx resolution better than 5% can be obtained at 35 samples. Fig. 13 exhibits a complete Gaussian spectrum for the truncated mean charge with an extracted dE/dx resolution of 4.9%. It should be noted that the trancated mean value (378 fC) is very close to the most probable value of the collected charge ($\approx$370 fC, see Fig. 10), showing that the Landau tail is almost removed completely by an 80% truncation with 35 samples.

The dE/dx resolution at different operating voltages is shown in Fig. 14. They are all better than 6% for high voltages of 2150, 2200 and 2250 V. The slightly better resolution is observed at higher operating voltages due to the larger gas amplification, which enhances the signal-to-noise ratio and reduces the fluctuation in the process of gas amplification.

5.5. Cell efficiency

Single cell efficiency is determined by the ratio of the number of hits in the cell to the number of tracks passing through the cell. Fig. 15 shows the cell efficiency averaged over all cells in each layer. All the layers have efficiencies higher than 97%, although at boundaries (including border

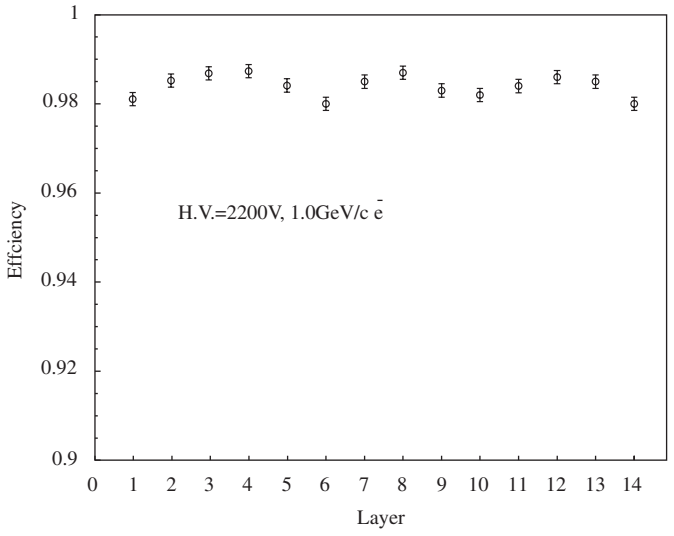

Fig. 15. Cell efficiency for each layer.

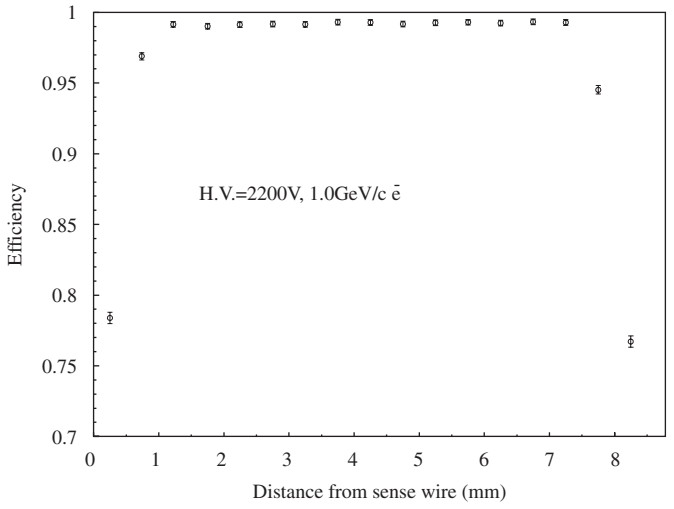

Fig. 16. Cell efficiency as a function of drift distance.

layers between neighboring super-layers) they are slightly lower due to the distortion of the electric field.

Cell efficiency is also a function of drift distance, as shown in Fig. 16, at a high voltage of 2200 V. The efficiency is well over 98% in the middle of the cell while drops sharply near the sense wire and the cell edge due to a very non-isochronic charge collection, which leads to the smaller signal with slow rise time.

Fig. 17 shows the cell efficiency averaged over all the cells at different operating voltages. It can be seen that the efficiencies at such operating voltages are over 98% and the minor improvement still can be obtained with an increase of the operating voltage.

6. Conclusions

A beam test of the full-length prototype with the electronics designed for the BESIII drift chamber was

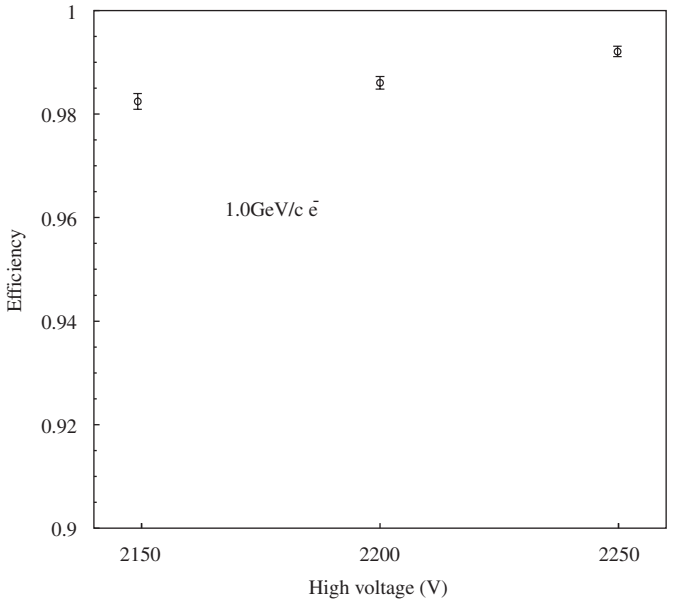

Fig. 17. Cell efficiency at different operating voltages.

carried out. During the test, the electronics system, especially the MQT module, worked successfully and its status was satisfied A good spatial resolution of 123 μm by using the "single-threshold method", and a better spatial resolution of 114 μm by using the "double-threshold method", were obtained at the high voltage of 2200 V. A dE/dx resolution of better than 5% and a cell efficiency of over 98% were also achieved at the same high voltage. These results verify the feasibility and validity of the design of the drift chamber and its readout electronics, and demonstrate their good performances. The BESIII drift chamber is expected to meet its design specifications, and the double threshold can deliver a better spatial resolution.

Acknowledgments

The authors would like to thank the test beam group for their great help throughout the entire test. The authors also thank the BEPC LINAC group for providing and monitoring the beam. This work is supported partly by the BEPCII/BESIII construction project and the Knowledge Innovation Project of Chinese Academy of Sciences under Contract nos. U-602 and U-34 (IHEP).

References

[1] BESIII Collaboration, BESIII Preliminary Design Report, 2004, 〈http://bes.ihep.ac.cn/bes3/design05/design/design1.htm〉.
[2] BEPCII Preliminary Design Report, 2002. 〈http://acc-center.ihep.ac.cn/download/pdr_download.htm〉.
[3] 〈http://micdigital.web.cern.ch/micdigital/hptdc.htm〉.
[4] 〈http://www.ihep.ac.cn/facility/testbeam/index-English.htm〉.
[5] L.H. Wu, et al., High Energy Phys. Nucl. Phys. 29 (2005) 476 (in Chinese).

[6] M.H. Xu, et al., Nucl. Electron. & Detect. Technol. 26 (2006) 199 (in Chinese).
[7] 〈http://www.caen.it/nuclear/syproduct.php?mod = SY127〉.
[8] D. Peterson, et al., Nucl. Instr. and Meth. A 478 (2002) 142.
[9] M. Adinolfi, et al., Nucl. Instr. and Meth. A 488 (2002) 51.
[10] V. Cindro, et al., Nucl. Instr. and Meth. A 309 (1991) 411.
[11] J.B. Liu, et al., Nucl. Instr. and Meth. A 557 (2006) 436.
[12] D. Jeanne, et al., Nucl. Instr. and Meth. A 111 (1973) 287.
[13] W. Allison, J. Cobb, Annu. Rev. Nucl. Part. Sci. 30 (1980) 253.